J. Fluid Mech. (1997), *vol.* 346, *pp.* 271–290. Printed in the United Kingdom

Nonlinear self-excited oscillations of a ducted flame

By A. P. DOWLING

Cambridge University Engineering Department, Trumpington Street, Cambridge CB2 1PZ, UK

(Received 24 July 1996 and in revised form 7 May 1997)

Self-excited oscillations of a confined flame, burning in the wake of a bluff-body flame-holder, are considered. These oscillations occur due to interaction between unsteady combustion and acoustic waves. According to linear theory, flow disturbances grow exponentially with time. A theory for nonlinear oscillations is developed, exploiting the fact that the main nonlinearity is in the heat release rate, which essentially 'saturates'. The amplitudes of the pressure fluctuations are sufficiently small that the acoustic waves remain linear. The time evolution of the oscillations is determined by numerical integration and inclusion of nonlinear effects is found to lead to limit cycles of finite amplitude. The predicted limit cycles are compared with results from experiments and from linear theory. The amplitudes and spectra of the limit-cycle oscillations are in reasonable agreement with experiment. Linear theory is found to predict the frequency and mode shape of the nonlinear oscillations remarkably well. Moreover, we find that, for this type of nonlinearity, describing function analysis enables a good estimate of the limit-cycle amplitude to be obtained from linear theory.

Active control has been successfully applied to eliminate these oscillations. We demonstrate the same effect by adding a feedback control system to our nonlinear model. This theory is used to explain why any linear controller capable of stabilizing the linear flow disturbances is also able to stabilize finite-amplitude oscillations in the nonlinear limit cycles.

1. Introduction

Combustion oscillations occur in the afterburners of aeroengines, where the associated pressure waves can become so intense that they do structural damage. These self-excited oscillations involve coupling between unsteady combustion and acoustic waves in the afterburner duct. Essentially, the velocity fluctuations associated with the acoustic waves perturb the flame and change the instantaneous rate of heat release. Since these fluctuations in heat release rate generate sound, the acoustic waves can gain energy from their interaction with the unsteady combustion (Rayleigh 1896). If this energy gain exceeds that lost on reflection at the ends of the duct, linear acoustic waves grow in amplitude until limited by nonlinear effects.

In an afterburner, the combustion is stabilized in the recirculation zone of a bluff body. Most laboratory models of afterburners consist of ducted flames stabilized in the wake of V-shaped flame-holders, baffles or rearward-facing steps (see, for example, Yamaguchi, Ohiwa & Hawegawa 1985; Sivasegaram & Whitelaw 1987; Schadow, Wilson & Gutmark 1988; Hedge, Reuter & Zinn 1988; Langhorne 1988). Schlieren visualizations of the flame have been made in a number of investigations (Smart,

Jones & Jewel 1976; Pitz & Daily 1981; Keller *et al.* 1982; Smith & Zukoski 1985; Sterling & Zukoski 1987; Poinsot *et al.* 1987). The review by Schadow & Gutmark (1992) gives a summary of these observations: flow unsteadiness at the flame-holder forces the shedding of large vortices, which perturb the flame front as they travel downstream, leading to time variations in the heat release rate. Similar effects are seen in the numerical simulations of Kailasanath *et al.* (1991). The response of a flame to flow unsteadiness is of crucial importance to the occurrence of acoustically coupled combustion oscillations.

Bloxsidge, Dowling & Langhorne (1988*b*) investigated this experimentally by exciting a stable confined flame with weak harmonic sound waves. They found that the unsteady burning was determined principally by velocity fluctuations at the flame-holder, and gave an empirical form for the relationship between linear fluctuations in heat release rate and flow velocity. They used this to develop a linear stability analysis for a flame burning in a duct. Their theory predicts frequencies and mode shapes which are in good agreement with Langhorne's (1988) low-Mach-number experimental data. This theory was subsequently applied successfully to flows with higher inlet Mach numbers (Macquisten & Dowling 1993) and more complex geometries (Macquisten & Dowling 1995).

However, linear theory predicts that flow perturbations grow exponentially in time and gives no information about the amplitude of the oscillations that would occur in practice. In this paper, we extend the flame model of Bloxsidge *et al.* (1988*b*) to include nonlinear effects. The theory exploits the fact that the main nonlinearity is in the velocity field and hence in the heat release rate. This is because, for the low-Mach-number flows appropriate to afterburners, the fractional velocity perturbation $u'/\bar{u}$ is much larger than the fractional pressure variation, $p'/\bar{p}$. In rig experiments, flow reversal has been observed during part of the oscillation cycle, leading to $u'/\bar{u} \sim O(1)$, even though the pressure perturbation is less than 10%. Measurements of the filtered light emission by C_2 radicals (see for example Macquisten & Dowling 1993, figure 4) show that large fluctuations in heat release rate occur, even though the pressure perturbation is small. Similar effects are seen in Poinsot & Candel's (1988) direct simulation of combustion oscillations. Therefore, although the acoustic waves are linear, nonlinear effects must be included in the relationship between the unsteady heat release rate and the flow velocity.

Since we wish to focus on the effects of nonlinearity, we simplify the spatial distribution in heat input by considering it concentrated at a single axial plane. Extension of the Bloxsidge *et al.* (1988*b*) flame model to include nonlinear effects is straightforward. For weak perturbations their model says that the instantaneous heat release rate $Q(t)$ lags the velocity at the flame holder, $u_1(t)$. For finite-amplitude oscillations, this relationship must 'saturate' when the flow velocity reverses.

In §2 we use such a nonlinear flame model, together with the equations of conservation of mass, momentum and energy across the flame zone and the duct boundary conditions, to determine the time evolution of disturbances in the duct. At fuel–air ratios at which linear theory predicts exponentially growing disturbances, the nonlinear theory leads to limit cycles whose amplitudes are in good agreement with Langhorne's (1988) low-Mach-number experimental data. By investigating the effect of noise in the system, we are able to explain the significant alteration observed experimentally in the power spectral density of the pressure perturbation as the fuel–air ratio increases.

Results from the linear and nonlinear theories are compared in §3. We find that the frequency and mode shape are well described by linear theory. Moreover, for this type of nonlinearity, in which the unsteady heat release rate saturates, describing

function analysis enables a good estimate of the limit-cycle amplitude to be obtained from linear theory.

There have been a number of successful demonstrations of the elimination of combustion instabilities by active control (Heckl 1988; Bloxsidge *et al.* 1988*a*; Poinsot *et al.* 1989; Langhorne, Dowling & Hooper 1990; Gulati & Mani 1990). A typical practical system uses a pressure transducer upstream of the flame zone to monitor the unsteady flow. This signal is time-delayed and used to drive an actuator which might be a loudspeaker, or other vibrating body, or fuel injectors. Provided the time delay and gain are suitably chosen the feedback controller can stabilize the flow.

In §4 we demonstrate the same effect by adding a feedback control system to our theoretical model. Describing function analysis is used to explain a puzzling feature of the experimental results: a feedback controller designed to stabilize linear disturbances is found to be equally effective at eliminating the nonlinear limit-cycle oscillation. Describing function analysis (sometimes called the theory of equivalent complex gains) is an approximate way of determining the nonlinear response to a single-frequency input. A complex transfer function between the output and input is defined, just as for a linear system, except now the transfer function depends on the input amplitude. Using describing function analysis, we obtain simple results for the form of nonlinearity in which the heat release rate essentially 'saturates'. We show that any linear controller capable of stabilizing linear flow disturbances is also able to stabilize the nonlinear limit cycle. A linear controller with a transfer function of the appropriate phase, but whose gain is less than that required to stabilize linear flow disturbances, just reduces the amplitude of the limit cycle. These predictions are confirmed by calculating the time history of the flow oscillations.

2. Nonlinear theory

Consider a confined premixed turbulent flame, stabilized in the wake of a V-shaped conical bluff body. This provides a generic model of an afterburner, and has been extensively investigated experimentally. Linear theories for the self-excited oscillations of such a flame are well-developed and lead to disturbances proportional to $e^{i\omega t}$ (see, for example, Bloxsidge *et al.* 1988*b*). For a range of fuel–air ratios, $\mathrm{Im}(\omega)$ is negative and linear disturbances are predicted to grow exponentially with time. We will include nonlinear effects in the modelling for the particular case when the main nonlinearity is in the combustion rate. Then finite-amplitude limit cycles develop.

Tien (1984) reviews a number of methods for analysing nonlinear combustion oscillations. The most commonly used is a Galerkin expansion which leads to a coupled set of ordinary differential equations for the time-varying coefficients of the Galerkin series (see, for example, Lores & Zinn 1973). These equations can be simplified by taking a short-time average. Culick (1988) summarizes this technique and applications of this method are described by Awad & Culick (1986) and Wicker, Yoon & Yang (1995). Simple estimates of growth rate and of the amplitude of the limit cycle can be obtained by an energy balance (e.g. Segawa 1980; Flandro 1985 and Yoon & Chung 1994). Usually in these methods the perturbation amplitude is treated as a small parameter and only terms up to second, or sometimes third, order are retained. We adopt a different approach, since we expect fluctuations in heat release rate and in velocity to be the same order as their mean. We just integrate in time and this is made easy by recognizing that the acoustic waves are still linear.

In practice, combustion is distributed along the duct downstream of the flame-holder. However, since our interest is in focusing on nonlinear effects, we will simplify

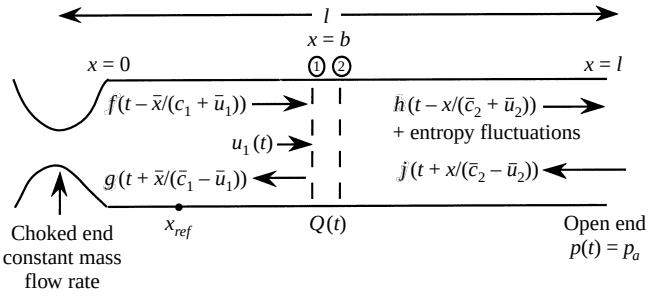

FIGURE 1. Schematic diagram of the geometry and flow.

the heat input by considering it concentrated over a short axial length. This may lead to some inaccuracy in the predicted frequency (Dowling 1995), but it makes the analysis sufficiently tractable to clarify the rôle of nonlinearities. We are interested in low frequencies of oscillation at which the acoustic wavelength is very long in comparison with the duct diameter. Therefore, only plane acoustic waves carry energy and higher-order modes decay exponentially fast with axial distance. We enclose the burning region by a control surface, whose axial length may extend several duct diameters, but is short in comparison with the acoustic wavelength. While the flame geometry and hence the flow within the control volume are two-dimensional, the acoustic waves outside the control surface revert to being one-dimensional and couple to the heat release rate integrated over the cross-section. The assumption that the combustion zone is short in comparison with the wavelength means that we can consider the heat input as concentrated at a single axial plane. Figure 1 shows a schematic diagram of the geometry and flow.

The Bloxsidge *et al.* (1988*b*) empirical flame model relates the instantaneous heat release rate $Q(t)$ to linear perturbations in $u_1(t)$, the flow velocity at the flame holder. They chose to work in the frequency domain. Although they give a complicated expression, for the frequency range of interest $\omega\tau_1 \gg 1$, their flame model (see Bloxsidge *et al.* 1988*b*, equation 3.9) leads to

$$\frac{\hat{Q}}{\bar{Q}} = \frac{1}{1 + \mathrm{i}\omega\tau_1} \frac{\hat{u}_1}{\bar{u}_1} \mathrm{e}^{-\mathrm{i}\omega\tau_2}. \tag{2.1}$$

The overbar denotes the mean value and the circumflex the complex amplitude of disturbances of frequency ω; τ_1 and τ_2 represent time delays. Bloxsidge *et al.* suggest $\tau_1 = 2\pi r_B(1-\alpha)/\bar{u}_1$, where r_B and α are the radius and blockage ratio of the flame-holder respectively. τ_2 is proportional to $(l-b)/\bar{u}_1$, where $l-b$ is the duct length downstream of the flame-holder shown in figure 1. Experiments at a range of different flow conditions have confirmed that the time delays involve convective (not diffusive) effects. The flow impedance at the flame has been altered by changing the inlet geometry (see, for example, Macquisten & Dowling 1995) to check that the unsteady heat release depends on local velocity fluctuations, and not on pressure as predicted when the flame is planar and aligned with the oncoming flow (McIntosh 1991).

In the time domain, the first-order differential equation (2.1) is equivalent to

$$\tau_1 \frac{\mathrm{d}Q}{\mathrm{d}t} + Q(t) = \frac{\bar{Q}}{\bar{u}_1} u_1(t - \tau_2), \tag{2.2}$$

for small-amplitude perturbations about a mean heat release rate $\bar{Q}$ and mean velocity $\bar{u}_1$ at the flame-holder. It is convenient to introduce the 'quasi-steady' or 'steady-state'

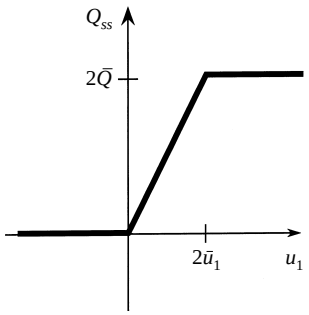

FIGURE 2. Nonlinear saturation form for $Q_{ss}(u_1)$.

heat release rate Q_{ss}. $Q_{ss}(u_1)$ is the rate of heat release that would occur in a flow whose velocity is constant and equal to the instantaneous velocity $u_1(t)$. For linear perturbations from $\bar{u}_1$, $Q_{ss}(u_1)$ is proportional to u_1 and we write

$$Q_{ss}(u_1) = \eta \Delta H \, A \bar{\rho}_1 u_1 \quad \text{for } u_1 \text{ near } \bar{u}_1. \tag{2.3}$$

η is the combustion efficiency, ΔH is the heat released/unit mass of premixed gas burnt and $\rho_1 A u_1$ is the mass flow rate into the burning region, ρ_1 being the density and A the duct area. Since $\bar{Q} = \eta \Delta H \, A \bar{\rho}_1 \bar{u}_1$, the right-hand side of (2.2) simplifies to $Q_{ss}(t - \tau_2)$, i.e.

$$\tau_1 \frac{\mathrm{d}Q}{\mathrm{d}t} + Q(t) = Q_{ss}(u_1(t - \tau_2)). \tag{2.4}$$

For slowly varying changes, it is evident from (2.4) that $Q(t)$ reduces to the steady-state heat release rate $Q_{ss}(u_1)$. When the fluctuations are more rapid, equation (2.4) describes a time lag and a reduction in amplitude between the heat release rate $Q(t)$ and its quasi-steady value. It is interesting to note that Fleifil *et al.* (1996) derive a lag law in a similar form to (2.2), but with $\tau_2 = 0$, for a wrinkled laminar flame tethered by a ring around the duct circumference. Similar lag laws have been used to describe flow disturbances in compressors (Greitzer 1976) and in diffusers (Kwong & Dowling 1994).

For nonlinear fluctuations, we continue to use equation (2.4) to determine the instantaneous heat release rate, but recognize that when the flow velocity reverses, $Q_{ss}(u_1)$ cannot become negative. The mean value of Q_{ss} must remain equal to $\eta \Delta H \, A \bar{\rho}_1 \bar{u}_1$, since η is the mean combustion efficiency. We therefore take $Q_{ss}(u_1)$ to have the saturation form illustrated in figure 2:

$$Q_{ss}(u_1) = \begin{cases} 0 & \text{for} \quad u_1 \leqslant 0 \\ \eta \Delta A \bar{\rho}_1 u_1 & \text{for} \quad 0 \leqslant u_1 \leqslant 2\bar{u}_1 \\ \eta \Delta A \bar{\rho}_1 2\bar{u}_1 & \text{for} \quad 2\bar{u}_1 \leqslant u_1. \end{cases} \tag{2.5}$$

Nonlinearity in (2.5) alters the unsteady heat input once the velocity perturbation $u_1'(t)$ exceeds $\bar{u}_1$. We expect oscillations in which $Q(t)$ and $u(x,t)$ vary in a nonlinear way, with fluctuations of the order of their mean.

The equations of continuity of mass, momentum and energy across the flame zone at $x = b$ can be written in the form

$$[\rho u]_1^2 = 0, \tag{2.6}$$

$$[p + \rho u^2]_1^2 = 0, \tag{2.7}$$

and

$$[(c_p T + \tfrac{1}{2}u^2)\rho u A]_1^2 = Q, \tag{2.8}$$

where the suffices 1 and 2 denote flow quantities at $x = b^-$ and b^+ respectively. Acoustic waves propagate upstream of the flame zone, while downstream both acoustic waves and entropy fluctuations occur. We want to relate the upstream and downstream acoustic waves to $Q(t)$. That can be done by combining (2.6)–(2.8), with the perfect gas equation, to obtain two equations, which are independent of ρ_2 and T_2.

The first of these equations follows directly from substitution of (2.6) into (2.7), and is

$$[p]_1^2 + \rho_1 u_1 [u]_1^2 = 0. \tag{2.9}$$

To obtain the second, we expand the left-hand side of the energy equation (2.8) in the form

$$[c_p T \rho u]_1^2 + [\rho u \tfrac{1}{2}u^2] = Q/A. \tag{2.10}$$

After using the perfect gas equation to rewrite $T\rho$ as p/R and replacing $\rho_2 u_2$ by $\rho_1 u_1$ from equation (2.6), this simplifies to

$$\frac{\gamma}{\gamma - 1}[pu]_1^2 + \rho_1 u_1 [\tfrac{1}{2}u^2] = Q/A, \tag{2.11}$$

where γ is the ratio of specific heat capacities.

In acoustic waves, $p' \sim O(u'\bar{\rho}\,\bar{c})$, where $\bar{c}$ is the speed of sound. Hence

$$\frac{p'}{\bar{p}} = O(\gamma \bar{M})\frac{u'}{\bar{u}}, \tag{2.12}$$

where $\bar{M}$ is the mean Mach number. For the low-Mach-number flows in an afterburner, the fractional pressure fluctuation remains small, even when $u'/\bar{u} \sim O(1)$. Since u' is also much less than $\bar{c}$, the acoustic waves can be treated as linear. Therefore, for the region upstream of the combustion zone, $0 \leqslant x \leqslant b$, we can write the flow variables in the form

$$p(x,t) = \bar{p}_1 + f\left(t - \frac{x-b}{\bar{c}_1 + \bar{u}_1}\right) + g\left(t + \frac{x-b}{\bar{c}_1 - \bar{u}_1}\right), \tag{2.13a}$$

$$u(x,t) = \bar{u}_1 + \frac{1}{\bar{\rho}_1 \bar{c}_1}\left(f\left(t - \frac{x-b}{\bar{c}_1 + \bar{u}_1}\right) - g\left(t + \frac{x-b}{\bar{c}_1 - \bar{u}_1}\right)\right), \tag{2.13b}$$

with

$$\rho(x,t) = \bar{\rho}_1 + \frac{1}{\bar{c}_1^2}\left(f\left(t - \frac{x-b}{\bar{c}_1 + \bar{u}_1}\right) + g\left(t + \frac{x-b}{\bar{c}_1 - \bar{u}_1}\right)\right). \tag{2.13c}$$

f and g denote the strength of the downstream- and upstream-propagating acoustic waves respectively, with their phase referenced from $x = b$.

In Langhorne's (1988) experiments, the inlet flow at $x = 0$ is choked, so that the mass flow rate is constant there. This boundary condition leads to a simple description of how an incoming wave is reflected:

$$f(t) = \frac{1 - \bar{M}_1}{1 + \bar{M}_1} g(t - \tau_u), \tag{2.14}$$

where $\bar{M}_1$ is the mean Mach number upstream of the burning zone and $\tau_u = 2b/\bar{c}_1(1 - \bar{M}_1^2)$.

Total length of working section, $l = 1.92$ m
Axial position of flame holder, $b = 1.18$ m
Diameter of duct $= 0.07$ m
Diameter of flame-holder, $2r_B = 0.035$ m
Flame-holder blockage ratio, $\alpha = 25\%$

TABLE 1. Summary of the geometry

The acoustic waves in the duct downstream of the burning zone are also linear. Neglecting the influence of the entropy fluctuations on the propagation speed and impedance of these waves, we obtain

$$p(x,t) = \bar{p}_2 + h\left(t - \frac{x-b}{\bar{c}_2 + \bar{u}_2}\right) + j\left(t + \frac{x-b}{\bar{c}_2 - \bar{u}_2}\right) \tag{2.15a}$$

and

$$u(x,t) = \bar{u}_2 + \frac{1}{\bar{\rho}_2 \bar{c}_2}\left(h\left(t - \frac{x-b}{\bar{c}_2 + \bar{u}_2}\right) - j\left(t + \frac{x-b}{\bar{c}_2 - \bar{u}_2}\right)\right) \tag{2.15b}$$

for $b \leqslant x \leqslant l$. Application of the open end boundary condition, $p'(l,t) = 0$, shows that

$$j(t) = -h(t - \tau_D), \tag{2.16}$$

where $\tau_D = 2(l-b)/\bar{c}_2(1-\bar{M}_2^2)$.

Substitution of (2.13)–(2.16) into (2.10) and (2.11) leads to two equations relating $g(t)$ and $h(t)$ to $Q(t)$ and their values at earlier times:

$$\boldsymbol{X}\begin{pmatrix} g(t) \\ h(t) \end{pmatrix} = \boldsymbol{Y}\begin{pmatrix} g(t-\tau_U) \\ h(t-\tau_D) \end{pmatrix} + \begin{pmatrix} 0 \\ (Q(t) - \bar{Q})/A\bar{c}_1 \end{pmatrix}. \tag{2.17}$$

τ_U and τ_D are the times taken for acoustic waves to travel up and down the regions upstream and downstream of the flame zone respectively. $\boldsymbol{X}$ and $\boldsymbol{Y}$ are 2×2 matrices, with constant coefficients just involving the mean flow. The full forms of $\boldsymbol{X}$ and $\boldsymbol{Y}$ are given in the Appendix.

The time evolution of the waves from specified initial conditions can now be determined in a straightforward way. If $g(t)$, $h(t)$ and $Q(t)$ are known up until a time t_1, integration of equation (2.4), with $Q_{ss}(t)$ from (2.5), leads to Q at the next time step $t_1 + \Delta t$. The values of $g(t_1 + \Delta t)$ and $h(t_1 + \Delta t)$ can be determined by using (2.17). Flow parameters in $0 \leqslant x \leqslant b$ then follow immediately from (2.13) and (2.14), and those in $b \leqslant x \leqslant l$ from (2.15) and (2.16). A fourth-order Runge–Kutta scheme was used for the numerical integration.

The geometry is summarized in table 1 and we first consider mean flow conditions corresponding to Langhorne's (1988) configuration 1: $\bar{M}_1 = 0.08$, $\bar{T}_{10} = 293$ K, equivalence ratio $\phi = 0.70$ (defined as the fuel–air ratio as a fraction of stoichiometric value). We will take the combustion efficiency $\eta = 0.80$ in all our calculations.

Integration of equation (2.4) in its current form leads to an unsteady flow dominated by a high-frequency combustion oscillation. However, in the experiment the frequency of the most unstable mode was 77 Hz, near the duct's fundamental frequency. Equations (2.1)–(2.3) were derived from low-frequency data (excitation in the range 15–95 Hz), and clearly overestimate the unsteady combustion that would be produced by forcing at much higher frequencies. For our purposes, therefore, we have modified this empirical flame model in a way that has negligible effect for the range of

frequencies at which it was measured, but leads to less unsteady heating at much higher frequencies. We take a second-order lag law of the form

$$\left(\tau_1 \frac{\mathrm{d}}{\mathrm{d}t} + 1\right)\left(\tau_3 \frac{\mathrm{d}}{\mathrm{d}t} + 1\right) Q(t) = Q_{ss}(u_1(t-\tau_2)). \tag{2.18}$$

Expansion of the left-hand side of (2.18) leads to

$$\left(1 + (\tau_1+\tau_3)\frac{\mathrm{d}}{\mathrm{d}t} + \tau_1\tau_3 \frac{\mathrm{d}^2}{\mathrm{d}t^2}\right) Q(t) = Q_{ss}(u_1(t-\tau_2)). \tag{2.19}$$

We choose the time constants in this equation from the Bloxsidge *et al.* (1988*b*) empirical form, and use a convective time delay $\tau_2 = 0.4(l-b)/\bar{u}_1$. The coefficient multiplying $\mathrm{d}Q/\mathrm{d}t$, $\tau_1+\tau_3$, is taken to be $2\pi r_B(1-\alpha)/\bar{u}_1$, the value given by Bloxsidge *et al.* τ_3 is to be sufficiently small that $\tau_1\tau_3\omega^2$ is negligible in comparison with $1 + \mathrm{i}\omega(\tau_1+\tau_3)$ at the frequencies at which Bloxsidge *et al.* measured the flame response (15–95 Hz). However, $\tau_1\tau_3\omega^2$ needs to be sufficiently large for frequencies near the third harmonic ($\sim$ 210 Hz) to reduce the amplitude of the predicted flame response at these frequencies. Within these constraints, the precise values of τ_1 and τ_3 are not important. In all our results, $\tau_1 = 5r_B(1-\alpha)/\bar{u}_1$ and $\tau_3 = 0.2\tau_1$.

Figure 3(*a*) shows small oscillations growing into a periodic, finite-amplitude oscillation. The pressure and velocity oscillations in this limit cycle are shown with an expanded timescale in figures 3(*b*) and 3(*c*). More information about these nonlinear periodic oscillations is given in the phase-space diagrams in figure 4. The fractional pressure perturbation remains small, the predicted r.m.s. pressure amplitude normalized on the mean pressure is 10.0%. This is in good agreement with the experimental nonlinear limit-cycle amplitudes reported by Langhorne (see Langhorne 1988, figure 5*b*). In the calculated oscillations, $u_1(t)$ is just negative during part of the cycle: the flow reversal seen experimentally is reproduced. There are large-amplitude variations in $Q(t)$, and $Q(t)$ is nearly zero for part of each cycle, again in agreement with experimental observations (Langhorne 1988, figure 11). For this inlet Mach number and temperature ($\bar{M}_1 = 0.08$, $\bar{T}_{10} = 293$ K), we find that linear disturbances are predicted to be unstable at all physically realisable, non-zero fuel–air ratios.

Results for a higher inlet temperature and Mach number ($\bar{T}_{10} = 460$ K, $\bar{M}_1 = 0.15$) are shown in figure 5. Experimental data for this case have been reported by Macquisten & Dowling (1993). Linear theory predicts that the instability onset occurs at $\phi = 0.69$, and the nonlinear results confirm this. The pressure time history in figure 5(*a*) is for $\phi = 0.60$ and oscillations ultimately decay, whereas for $\phi = 0.80$ in figure 5(*b*), linear perturbations grow into finite-amplitude cycles.

Afterburners are in a noisy environment and this was deliberately simulated in Langhorne's (1988) and Macquisten & Dowling's (1993) rig experiments, where there was a separated flow near the inlet and turbulence levels were typically 10%. We can investigate the response of our model to noise by forcing it by an incoming pressure disturbance $i(t)$ at $x = 0$. This leads to an extra term $i(t-\tau_B)$ on the right-hand side of (2.14), and to the additional term

$$\begin{pmatrix} 1 + \bar{M}_1\left(2 - \dfrac{\bar{u}_2}{\bar{u}_1}\right) + \bar{M}_1^2\left(1 - \dfrac{\bar{u}_2}{\bar{u}_1}\right) \\ \dfrac{1+\gamma\bar{M}_1}{\gamma-1} + \bar{M}_1^2 - \bar{M}_1^2(1+\bar{M}_1)^{\frac{1}{2}}\left(\dfrac{\bar{u}_2^2}{\bar{u}_1^2} - 1\right) \end{pmatrix} \mathrm{i}(t-\tau_B) \tag{2.20}$$

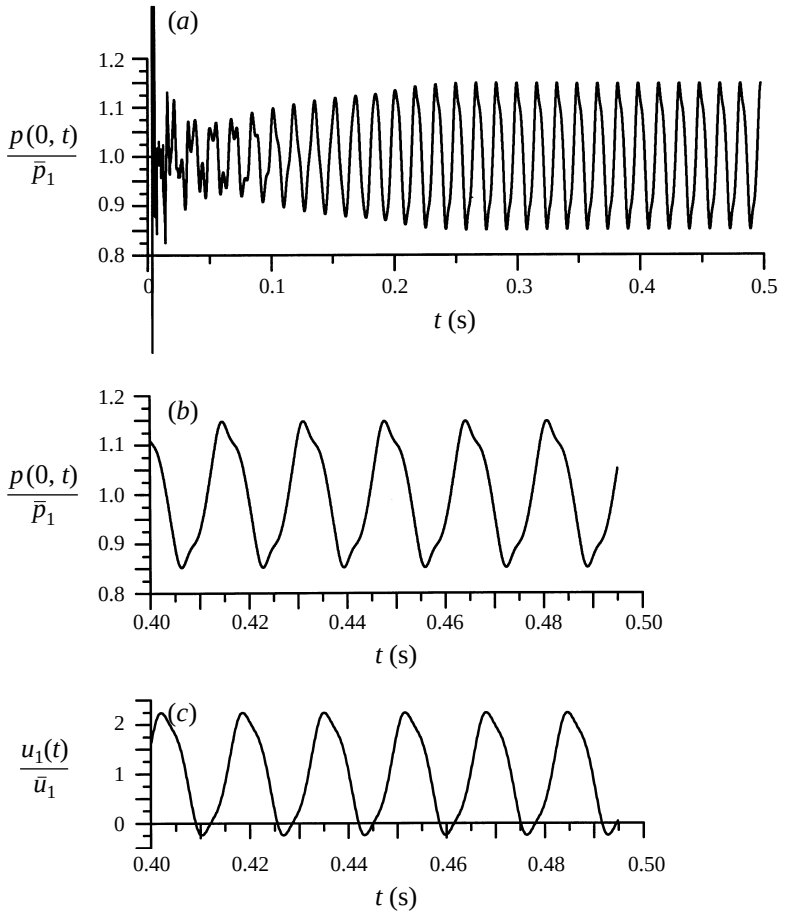

FIGURE 3. History of oscillations, $\bar{M}_1 = 0.08$, $\bar{T}_{10} = 293$ K, $\phi = 0.70$.

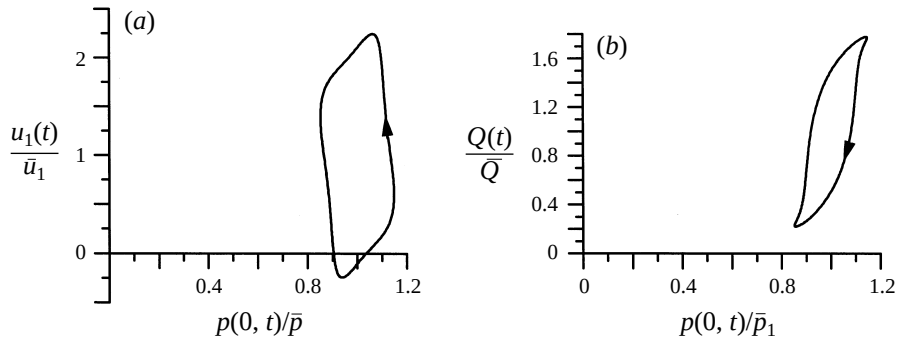

FIGURE 4. Phase-space diagrams, for $0.4 \leqslant t \leqslant 0.5$ s, $\bar{M}_1 = 0.08$, $\bar{T}_{10} = 293$ K, $\phi = 0.70$.

on the right-hand side of (2.17). $\tau_B = x_B/\bar{c}_1(1 - \bar{M}_1)$. For a specified noise function, $i(t)$, the numerical solution then proceeds as before.

Statistically stationary incoming noise leads to statistically stationary disturbances in the duct, even for the stable flow in figure 5(*a*). We have chosen to model $i(t)$ by a random distribution of discrete short-duration pulses. This has the advantage that

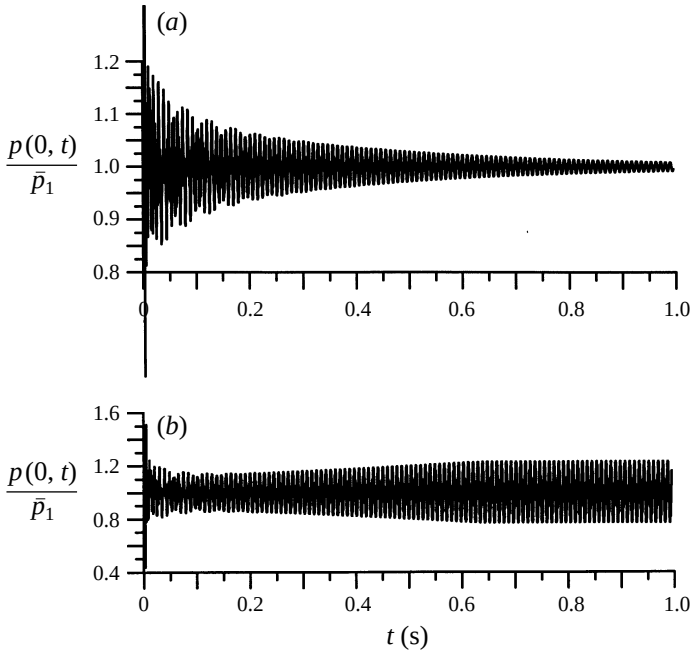

FIGURE 5. History of pressure oscillations, $\bar{M}_1 = 0.15$, $\bar{T}_{10} = 460$ K, (*a*) $\phi = 0.60$, (*b*) $\phi = 0.80$.

its power spectral density is effectively white (see figure 6*a*). The damped harmonic system in figure 5(*a*) responds to noise preferentially near its resonant frequency. This is seen clearly in the pressure spectra in figure 6(*b*). Even when the combustion oscillations of the ducted flame are stable, in a noisy system, there is a peak in the spectra at the frequency of the damped resonant mode. As the fuel–air ratio is increased and the flame becomes less stable, the damping factor is reduced and the height of the peak gradually increases. Throughout the range of stable fuel–air ratios, the pressure perturbation is directly proportional to the noise. However, for fuel–air ratios above the onset value, when the flow is unstable, the amplitudes of oscillation increase to those of the finite limit cycle. This results in a stronger, narrower peak in the spectrum, almost uninfluenced by noise (see figure 6*c*). The comparison with the experimental data in figure 7 is good. In particular, a similar change in the power spectral density with increasing fuel–air ratio is seen in the experimental results.

Although our nonlinear model is simple, it is able to reproduce the main features of the experimental limit cycles and the significant alteration in the pressure spectrum as the fuel–air ratio increases. It explains the abrupt increase in the amplitude of the fluctuations at a 'transition' fuel–air ratio as for example reported by Langhorne (see Langhorne 1988, figure 5*b*).

3. Comparison between linear and nonlinear theory

For linear fluctuations each Fourier mode can be considered independently, and so it is sufficient just to investigate perturbations with time dependence $e^{i\omega t}$. Disturbances only satisfy the equations of fluid motion and the duct boundary conditions for certain discrete complex values of ω, the eigenfrequencies: $\mathrm{Im}(\omega)$ describes the growth or decay of linear disturbances, while $\mathrm{Re}(\omega)$ gives the frequency of oscillation. Previous work has shown that the predicted frequencies are in good agreement with the

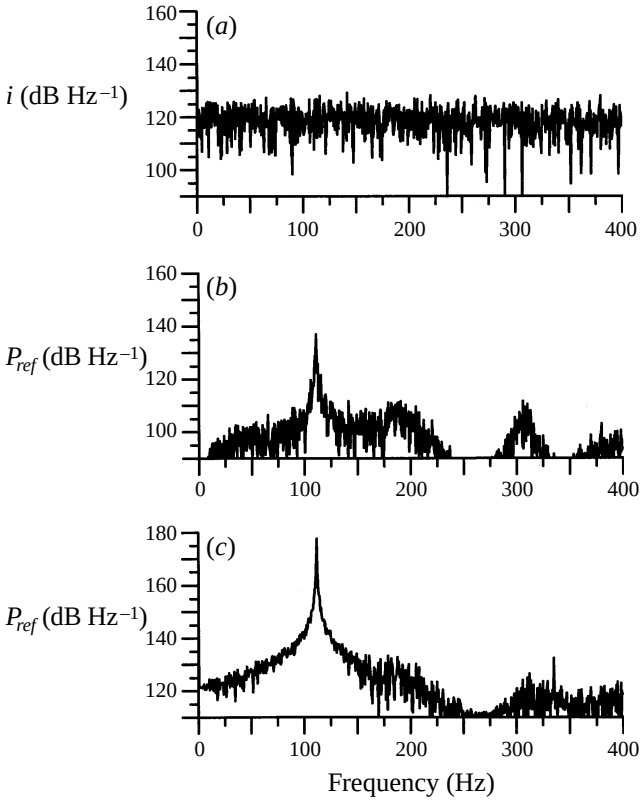

FIGURE 6. Calculated power spectral densities of (*a*) $i(t)$ and (*b*, *c*) $p(x_{ref}, t)$, $x_{ref} = 1.48$ m, $\bar{M}_1 = 0.15$, $\bar{T}_{10} = 460$ K, (*b*) $\phi = 0.60$, (*c*) $\phi = 0.80$.

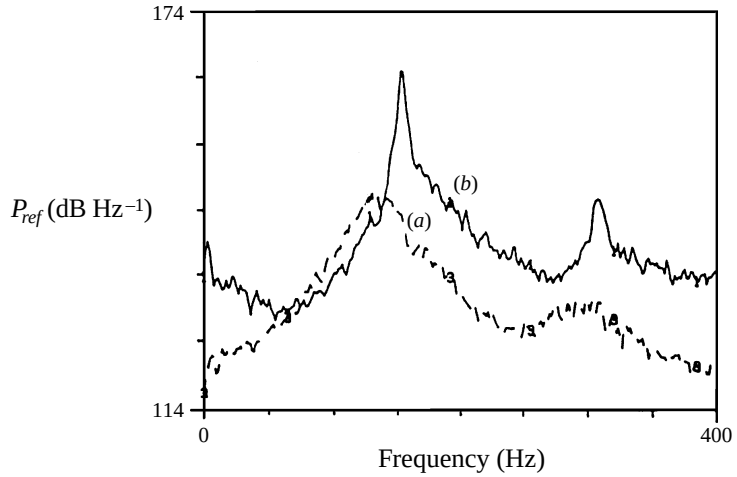

FIGURE 7. Experimental power spectral density of $p(x_{ref}, t)$, $x_{ref} = 1.48$ m, $\bar{M}_1 = 0.15$, $\bar{T}_{10} = 460$ K, (*a*) $\phi = 0.73$, (*b*) $\phi = 0.78$ (Macquisten, unpublished data).

experimental frequencies of oscillation. Mode shapes predicted from linear theory have also been found to agree well with measurements. In this section, we investigate why linear theory is so successful, by seeing how nonlinearity affects calculated frequencies and mode shapes.

For disturbances proportional to $e^{i\omega t}$, equation (2.17) simplifies to

$$\left(\boldsymbol{X} - \boldsymbol{Y}\begin{pmatrix} e^{-i\omega\tau_U} & 0 \\ 0 & e^{-i\omega\tau_D} \end{pmatrix}\right)\begin{pmatrix} \hat{g}(\omega) \\ \hat{h}(\omega) \end{pmatrix} = \begin{pmatrix} 0 \\ \hat{Q}(\omega)/A\bar{c}_1 \end{pmatrix}. \tag{3.1}$$

This can be readily solved to relate $\hat{g}(\omega)$ and $\hat{h}(\omega)$ to $\hat{Q}(\omega)/A\bar{c}_1$; $\hat{u}_1(\omega)$ then follows from (2.13*b*) and (2.14) and we write it in the form

$$\hat{u}_1(\omega) = \hat{G}(\omega)\hat{Q}(\omega)/A\bar{\rho}_1\bar{c}_1^2. \tag{3.2}$$

The function $\hat{G}(\omega)$ calculated in this way is the transfer function between velocity fluctuations at the flame-holder and unsteadiness in heat release rate. It essentially describes the generation of acoustic waves by unsteady heat input and depends on the duct geometry, mean flow and sound speed.

For linear perturbations proportional to $e^{i\omega t}$, the flame model defined through (2.5) and (2.18) simplifies to

$$\hat{Q}(\omega)/A\bar{\rho}_1\bar{c}_1^2 = -\hat{H}(\omega)\hat{u}_1(\omega), \tag{3.3}$$

where

$$\hat{H}(\omega) = -\frac{\eta\Delta H}{\bar{c}_1^2}\,\frac{e^{-i\omega\tau_2}}{(i\omega\tau_1+1)(i\omega\tau_3+1)}. \tag{3.4}$$

Combining (3.2) and (3.3) leads to the characteristic equation for the eigenfrequency. We obtain

$$\hat{u}_1(\omega)(1 + \hat{G}(\omega)\hat{H}(\omega)) = 0. \tag{3.5}$$

Only disturbances whose frequency is a zero of $1+\hat{G}(\omega)\hat{H}(\omega)$ can exist as eigenmodes of the duct/flame geometry. Once the frequency of oscillation has been determined, the pressure mode shape and its relationship to $\hat{Q}$ can be calculated from (2.13)–(2.16) and (3.1).

For the case in figure 3, this linear theory predicts oscillations of frequency 60.7 Hz, with growth rate 5.9 s^{-1}. This is indistinguishable from the nonlinear limit-cycle frequency, as are the linear and nonlinear pressure mode shapes. The phases of the transfer function between pressure and heat release rate are also virtually identical. Saturation causes the amplitude of the nonlinear unsteady heat release rate to be slightly smaller than that from linear theory:

$$\text{linear}\frac{\hat{Q}}{\hat{p}(0)} = 328e^{i32^\circ},\ \text{nonlinear}\frac{\hat{Q}}{\hat{p}(0)} = 317e^{i32^\circ}. \tag{3.6}$$

Rayleigh (1896) gave a clear physical interpretation of the interaction between unsteady heating and acoustic waves. He noted that acoustic waves gain energy from unsteady combustion if the fluctuating heat release rate is, on average, in phase with the pressure perturbation. That result was put on a more mathematical basis by Chu (1964), who identified $E_G = (\gamma-1)\overline{p'Q'}/\bar{\rho}_1\bar{c}_1^2$ as the rate at which acoustic waves gain energy from unsteady combustion. For linear disturbances, E_G is proportional to the square of the amplitude of the perturbations. But, for finite-amplitude disturbances in which the flow velocity reverses, E_G increases less rapidly with amplitude. The acoustic waves remain linear even for these nonlinear oscillations. Hence E_L, the

rate at which acoustic energy is lost on reflection at the ends of the duct, is always proportional to the square of the amplitude of the perturbation. When the duct/flame arrangement is unstable, $E_G > E_L$, for linear perturbations. The amplitude of these linear disturbances therefore increases with time. Once saturation occurs, E_L increases more rapidly with amplitude than E_G. In the nonlinear limit cycle, there is no further change in amplitude. Hence $E_G = E_L$ and this energy balance determines the amplitude of the limit-cycle oscillation. Since the limit-cycle amplitudes are controlled by such a simple effect it is worth seeing whether linear theory can give useful information about their magnitudes.

We will use describing function analysis as described, for example, in Ogata (1970, Chap. 11) to develop a quasi-linear theory to estimate the limit-cycle amplitudes. These predictions will then be compared with results from the full nonlinear theory.

Even for nonlinear oscillations, the acoustic waves are still linear and are described by (3.1) and (3.2). The nonlinearity occurs in the relationship between the rate of heat release and velocity fluctuations at the flame-holder.

Consider a harmonic variation in the flow velocity at the flame-holder,

$$u_1(t) = \bar{u}_1(1 + V\cos\omega t), \tag{3.7}$$

i.e. V is the amplitude of the velocity perturbation non-dimensionalized on the mean velocity $\bar{u}_1$. When $V > 1$, $Q_{ss}(t)$ saturates during part of the cycle (see (2.5)). Although $Q_{ss}(t)$ is no longer harmonic, it is still periodic and can be expanded as a Fourier series:

$$Q_{ss}(t) = \eta\Delta H A\bar{\rho}_1\bar{u}_1\left(1 + V\sum_{n=1}^{\infty} a_n(V)\cos(n\omega t)\right), \tag{3.8}$$

where, in particular,

$$a_1(V) = \begin{cases} 1 & \text{if} \quad V < 1 \\ \dfrac{2}{\pi}\left(\sin^{-1}\left(\dfrac{1}{V}\right) + \dfrac{1}{V}\left(1 - \dfrac{1}{V^2}\right)^{\frac{1}{2}}\right) & \text{if} \quad V > 1. \end{cases} \tag{3.9}$$

Substitution for $Q_{ss}(t - \tau_2)$ into (2.19) leads to a similar Fourier series for $Q(t)$:

$$Q(t) = \eta\Delta H A\bar{\rho}_1\bar{u}_1 + \mathrm{Re}(\hat{Q}(\omega)\mathrm{e}^{\mathrm{i}\omega t}) + \text{higher frequency terms.} \tag{3.10}$$

$\hat{Q}(\omega)$ can be written in the form

$$\hat{Q}(\omega)/A\bar{\rho}_1\bar{c}_1^2 = -a_1(V)\hat{H}(\omega)\hat{u}_1(\omega), \tag{3.11}$$

where $\hat{H}(\omega)$ is the function defined in (3.4). The gain $a_1(V)$ is unity for linear disturbances, but is reduced for finite-amplitude disturbances as described by (3.9). The time derivative on the left-hand side of (2.2) means that the flame acts like a low-pass filter. The most important unsteady contribution to $Q(t)$ is therefore that from the lowest frequency ω. The response of $Q(t)$ to the higher-frequency terms in Q_{ss} is negligible.

A comparison of (3.3) and (3.11) shows that the response in heat release rate due to nonlinear velocity fluctuations is identical in form to that due to linear perturbations, except that saturation has reduced the amplitude of the response by the factor $a_1(V)$ defined in (3.9).

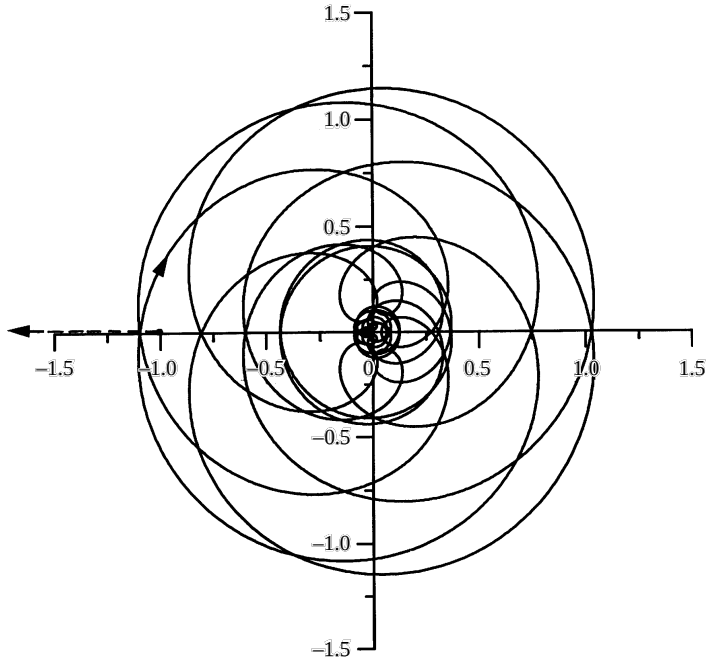

FIGURE 8. Nyquist stability curves for $\bar{M}_1 = 0.08$, $\bar{T}_{10} = 293$ K, $\phi = 0.7$: ———, locus of $\hat{G}(\omega)\hat{H}(\omega)$, $-\infty \leqslant \omega \leqslant \infty$, ω real; — — —, locus of $-[a_1(V)]^{-1}$, $0 \leqslant V \leqslant \infty$.

Combining (3.2) and (3.11), we obtain the characteristic equation for quasi-linear oscillations:

$$\frac{1}{a_1(V)} + \hat{G}(\omega)\hat{H}(\omega) = 0. \tag{3.12}$$

Oscillations of magnitude $\bar{u}_1 V$ grow in time, if this equation has any roots with $\mathrm{Re}(\mathrm{i}\omega) > 0$, whereas, if all the roots have $\mathrm{Re}(\mathrm{i}\omega) < 0$, the perturbations decrease.

The roots of (3.12) are most conveniently investigated by plotting the Nyquist curve for $\hat{G}(\omega)\hat{H}(\omega)$ and the locus of $-[a_1(V)]^{-1}$, $0 \leqslant V \leqslant \infty$. These are shown in figure 8 for the case $\bar{M}_1 = 0.08$, $\bar{T}_{10} = 293$ K, $\phi = 0.70$. The Nyquist curve crosses the negative real axis at $\hat{G}\hat{H} = -1.10$, and $[a_1(1.22)]^{-1} = 1.10$. This means that, for an oscillation whose non-dimensional amplitude V is less than 1.22, $[a_1(V)]^{-1}$ is smaller than 1.10. The Nyquist curve therefore encircles $-[a_1(V)]^{-1}$. Since there is then an unstable root, the disturbance grows in magnitude, increasing V and so moving $-[a_1(V)]^{-1}$ to the left. In a similar way, the Nyquist curve shows that any oscillation with V greater than 1.22 is stable and decays in amplitude, moving $-[a_1(V)]^{-1}$ to the right. Since any disturbance whose amplitude is less than 1.22 grows, while one whose amplitude is greater than 1.22 decays, in the limit-cycle we must have $V = 1.22$. In other words, the limit-cycle amplitude and frequency of oscillation ω are given by the value of V, which makes ω, the root of equation (3.12), real. In this example this corresponds to a peak-to-peak velocity fluctuation of $2.44\bar{u}_1$ in the velocity at the flame-holder at a frequency of 60.8 Hz, in excellent agreement with $2.49\bar{u}_1$ at 60.5 Hz calculated from the full nonlinear theory and shown in figures 3(*c*) and 4(*a*).

4. Feedback control

Active control has been demonstrated to be effective at reducing the oscillations of a ducted flame. In experiments the feedback controller was designed using standard control theory to stabilize linear perturbations of a flame, which would be unstable without control. However, the controller was found to be equally effective at eliminating the nonlinear limit-cycle oscillation. We can demonstrate the same effect with our model, and use describing function analysis to explain the controller's influence on the nonlinear limit cycle.

We will consider the simple control system used by Langhorne *et al.* (1990), in which additional fuel is injected unsteadily into the burning region. The pressure perturbation at a position x_{ref} is amplified by a gain k, delayed by a time interval τ and then used as the input into the control fuel injection system. This system inevitably has mass, stiffness and damping and we model it by assuming that $Q_C(t)$, the additional fluctuation in heat release rate produced by the controller, is related to the input signal, $p'(x_{ref}, t)$ through a second-order differential equation:

$$\left(\frac{1}{\omega_c^2}\frac{\mathrm{d}^2}{\mathrm{d}t^2} + \frac{2c}{\omega_c}\frac{\mathrm{d}}{\mathrm{d}t} + 1\right) Q_C(t) = k\frac{\eta \Delta H A}{\bar{c}_1} p'(x_{ref}, t-\tau). \tag{4.1}$$

ω_c and c are respectively the resonance frequency and damping of the control fuel injection system. The feedback gain k and time delay τ are to be chosen to stabilize the system.

The total heat input is

$$Q(t) = Q_N(t) + Q_C(t), \tag{4.2}$$

where $Q_N(t)$ now describes the naturally occurring heat release and is given by the solution of (2.18). $Q_C(t)$, the additional rate of heat release due to the controller, is given by the solution of (4.1). The other equations in §§2 and 3 are unaltered by control, but the function $Q(t)$ in (2.11) and (2.17) now refers to the total heat release rate, $Q_N(t) + Q_C(t)$, and similarly $\hat{Q}(\omega)$ in (3.2) is to be replaced by $\hat{Q}_N(\omega) + \hat{Q}_C(\omega)$.

We will first describe how control theory can be applied to determine the time delay τ and feedback gain k required to stabilize linear disturbances. It is appropriate to work in the frequency domain. Perturbations in flow velocity are caused by the total heat input, and writing $\hat{Q}(\omega) = \hat{Q}_N(\omega) + \hat{Q}_C(\omega)$ in (3.2) leads to

$$\hat{u}_1(\omega) = \hat{G}(\omega)\left(\hat{Q}_N(\omega) + \hat{Q}_C(\omega)\right) \Big/ A\bar{\rho}_1\bar{c}_1^2. \tag{4.3}$$

For linear disturbances, the flame model in (3.3) gives

$$\hat{Q}_N(\omega) \Big/ A\bar{\rho}_1\bar{c}_1^2 = -\hat{H}(\omega)\hat{u}_1(\omega), \tag{4.4}$$

where the function $\hat{H}(\omega)$ is defined in (3.4). The Fourier transform of (4.1) leads to

$$\hat{Q}_C(\omega) \Big/ A\bar{\rho}_1\bar{c}_1^2 = -k\hat{K}(\omega)\hat{u}_1(\omega), \tag{4.5}$$

where

$$\hat{K}(\omega) = -\frac{\eta \Delta H}{\bar{\rho}_1\bar{c}^3} \frac{\mathrm{e}^{-\mathrm{i}\omega\tau}}{1 + 2\mathrm{i}c(\omega/\omega_c) - (\omega/\omega_c)^2} \frac{\hat{p}(x_{ref}, \omega)}{\hat{u}_1(\omega)}.$$

After combining (4.3)–(4.5), we find that the eigenfrequencies of the controlled system are given by the roots of

$$1 + \hat{G}(\omega)(\hat{H}(\omega) + k\hat{K}(\omega)) = 0, \tag{4.6}$$

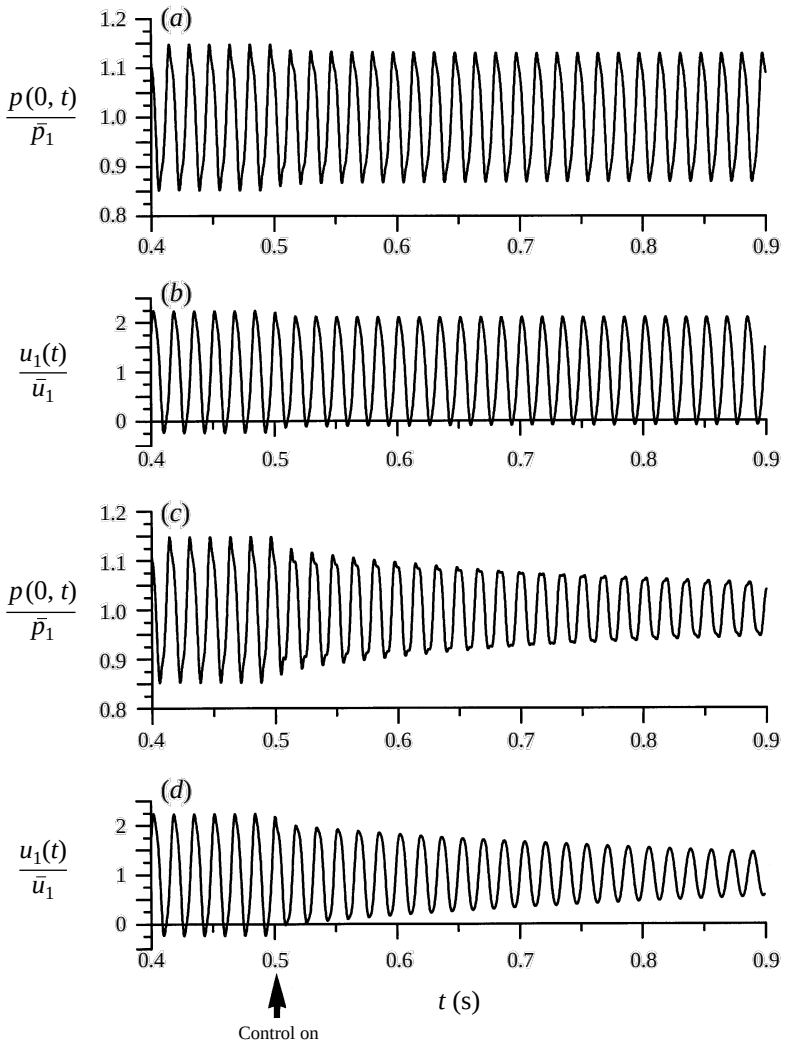

FIGURE 9. The effect of a controller switched on at $t = 0.5$ s, $\bar{M}_1 = 0.08$, $\bar{T}_{10} = 293$ K, $\phi = 0.7$, $x_{ref} = 0.75$ m, $\tau = 3$ ms: (*a*) and (*b*) $k = 0.10$, (*c*) and (*d*) $k = 0.20$.

which we rearrange as

$$k + \frac{1 + \hat{G}(\omega)\hat{H}(\omega)}{\hat{G}(\omega)\hat{K}(\omega)} = 0. \tag{4.7}$$

For stability, all the roots of this equation must have $\mathrm{Im}(\omega) > 0$. When $k = 0$, the lowest-frequency mode is unstable. Investigating the influence of small positive k, for various values of τ, shows that a controller with $\tau = 3$ ms tends to have a stabilizing effect. Plotting the Nyquist curve for $\tau = 3$ suggests that stability is achieved for $k \geqslant 0.16$. This was confirmed by calculating the roots of (4.7). For $k = 0.15$, the fundamental was found to have $\mathrm{Im}(\omega) < 0$ (unstable), for $k = 0.16$, $\mathrm{Im}(\omega) > 0$ (stable). Linear disturbances are stabilized once the gain k exceeds 0.16. We will denote this value of gain for stability of linear disturbances by k_l.

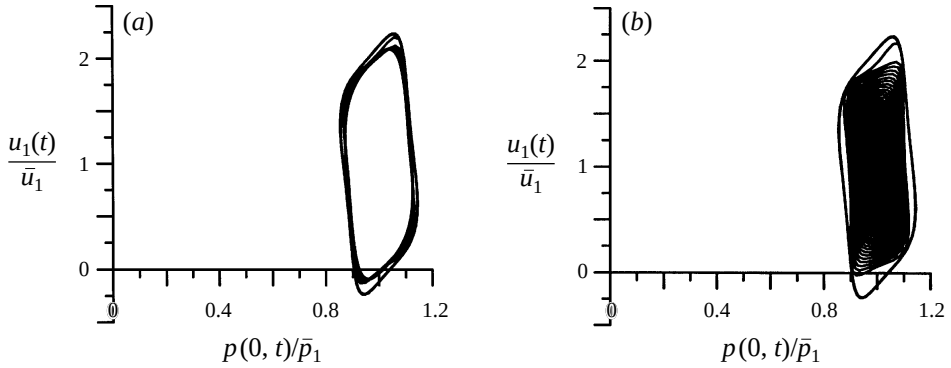

FIGURE 10. Phase-space diagrams for $0.4 \leqslant t \leqslant 4.0$ s, conditions as in figure 9. (*a*) $k = 0.10$, (*b*) $k = 0.20$.

The effects of such a controller on the finite-amplitude limit cycles can be determined by integration of (2.18) and (4.1) to obtain $Q(t) = Q_N(t) + Q_C(t)$. The evolution of the acoustic waves follows from (2.15) and the solution of (2.17), just as in §2. Typical results are shown in figure 9. The mean flow in figure 9 is identical to that in figure 3; $\bar{M}_1 = 0.08$, $\bar{T}_{10} = 293$ K, $\phi = 0.70$. To obtain these plots, the calculations in §2 were first run until a nonlinear limit cycle was established. The controller was then switched on at time $t = 0.5$ s. We find that for $k = 0.10 < k_l$, a new limit cycle of reduced amplitude is produced. But for $k = 0.2 > k_l$, the limit-cycle amplitude ultimately decays to zero. This is seen more clearly in the phase-space diagrams in figure 10. In §3, we found that describing function analysis gave good estimates of the limit-cycle amplitudes. The same theory can be used to explain the effects of the controller.

When the velocity at the flame holder undergoes a finite-amplitude oscillation as (3.7), equation (3.11) replaces (4.4) as a description of the flame response

$$\hat{Q}_N(\omega)/A\bar{\rho}_1\bar{c}_1^2 = -a_1(V)\hat{H}(\omega)\hat{u}_1(\omega), \tag{4.8}$$

where $a_1(V)$ is given in (3.9). After combining equations (4.3), (4.5) and (4.8), we find that the eigenfrequencies of the controlled nonlinear system are given by the roots of

$$1 + \hat{G}(\omega)\left(a_1(V)\hat{H}(\omega) + k\hat{K}(\omega)\right) = 0, \tag{4.9}$$

which we arrange as

$$\frac{1}{a_1(V)} + \frac{\hat{G}(\omega)\hat{H}(\omega)}{1 + k\hat{G}(\omega)\hat{K}(\omega)} = 0, \tag{4.10}$$

in order to use describing function analysis. Just as in §3, the stability and limit-cycle amplitudes can be conveniently investigated by plotting the Nyquist curve of

$$\hat{X}(\omega) = \frac{\hat{G}(\omega)\hat{H}(\omega)}{1 + k\hat{G}(\omega)\hat{K}(\omega)} \tag{4.11}$$

and the locus of $[a_1(V)]^{-1}$, for $0 \leqslant V \leqslant \infty$. For $k = 0$, this corresponds to the no control case in figure 8. Then the system is linearly unstable, with a peak-to-peak limit-cycle amplitude of $2\bar{u}_1 V = 2.44\bar{u}_1$. When k is increased to 0.1 (see figure 11*a*), the Nyquist curve crosses the negative real axis at -1.03. Linear perturbations are still unstable. Describing function analysis gives the non-dimensional limit-cycle amplitude V as the root of $[a_1(V)]^{-1} = 1.03$. The solution to this equation is $V = 1.09$, i.e. a

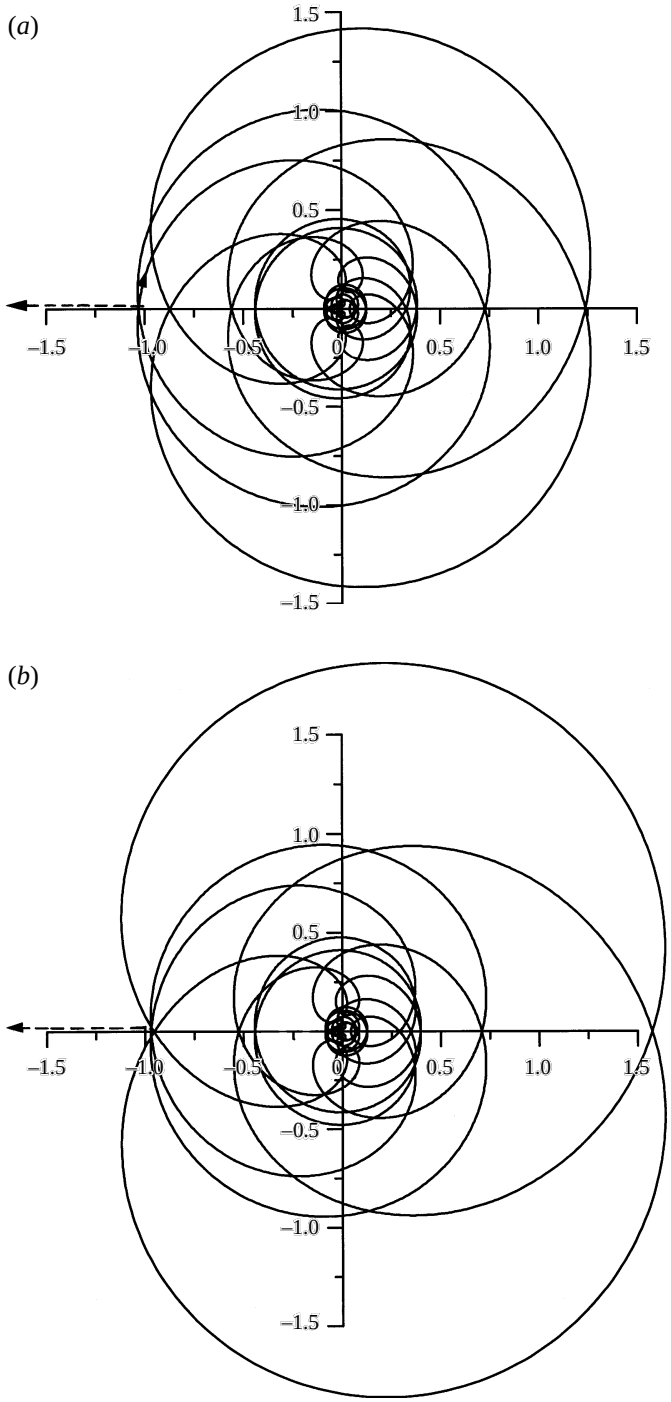

FIGURE 11. Nyquist stability curves with control. $\bar{M}_1 = 0.08$, $\bar{T}_{10} = 293$ K, $\phi = 0.7$, $x_{ref} = 0.75$ m, $\tau = 3$ ms: ———, locus of $\hat{X}(\omega)$ in equation (4.11), $-\infty \leqslant \omega \leqslant \infty$, ω real; – – –, locus of $-[a_1(V)]^{-1}$, $0 \leqslant V \leqslant \infty$, (*a*) $k = 0.10$, (*b*) $k = 0.20$.

peak-to-peak velocity fluctuation of $\bar{u}_1 = 2.19$, which is in excellent agreement with that calculated from the full nonlinear theory in figure 9(*b*). Finally in figure 11(*b*), k is greater than k_l, the gain required for stability of linear disturbances. The Nyquist curve therefore does not encircle -1. For finite-amplitude disturbances, $-[a_1(V)]^{-1}$ is to the left of -1, and so is certainly not encircled by the Nyquist curve. Disturbances of any amplitude therefore decay. The controller is even able to stabilize nonlinear oscillations as we saw in the time history plots in figures 9(*c*), 9(*d*) and 10(*b*).

Describing function analysis shows that the results we found from the nonlinear theory, for particular values of the gain k, apply more generally. A controller of fixed gain k capable of eliminating linear perturbations can also drive the nonlinear limit-cycle oscillations to zero. This is because the nonlinearity is due to 'saturation' in the heat release rate and the control task for finite amplitude V is actually easier than that for infinitesimal disturbances. A controller with a transfer function of the appropriate phase, but whose gain is less than that required to stabilize linear flow disturbances, just reduces the amplitude of the limit cycle.

5. Conclusions

The main nonlinearity in the oscillation of a flame burning in a duct is due to 'saturation' in the heat release rate. A theory based on this can lead to limit cycles, amplitudes and spectra in good agreement with experiment. This theory is also able to explain why linear theory can give good predictions for the frequency of oscillation and the mode shape. We have demonstrated how describing function analysis enables reasonable predictions for the limit-cycle amplitudes to be obtained from a quasi-linear theory.

This model has been used to explain why, for this type of nonlinearity, any linear controller of fixed gain capable of stabilizing linear flow perturbations can also stabilize the nonlinear limit cycles. A controller whose transfer function has the appropriate phase but whose gain is less than that required to stabilize linear flow disturbances, just reduces the limit-cycle amplitude.

Appendix

The full forms of the 2×2 matrices in equation (2.15) are

$$\boldsymbol{X} = \begin{pmatrix} -1 + \bar{M}_1\left(2 - \dfrac{\bar{u}_2}{\bar{u}_1}\right) - \bar{M}_1^2\left(1 - \dfrac{\bar{u}_2}{\bar{u}_1}\right) & 1 + \bar{M}_1 \dfrac{\bar{\rho}_1 \bar{c}_1}{\bar{\rho}_2 \bar{c}_2} \\ \dfrac{1 - \gamma \bar{M}_1}{\gamma - 1} + \bar{M}_1^2 - \bar{M}_1^2\,(1 - \bar{M}_1)\,\tfrac{1}{2}\left(\dfrac{\bar{u}_2^2}{\bar{u}_1^2} - 1\right) & \dfrac{\bar{c}_2}{\bar{c}_1}\,\dfrac{(1 + \gamma \bar{M}_2)}{\gamma - 1} + \bar{M}_1 \bar{M}_2 \dfrac{\bar{\rho}_1}{\bar{\rho}_2} \end{pmatrix},$$

$$\boldsymbol{Y} = \begin{pmatrix} \dfrac{1 - \bar{M}_1}{1 + \bar{M}_1}\left(1 + \bar{M}_1\left(2 - \dfrac{\bar{u}_2}{\bar{u}_1}\right) + \bar{M}_1^2\left(1 - \dfrac{\bar{u}_2}{\bar{u}_1}\right)\right) & 1 - \bar{M}_1 \dfrac{\bar{\rho}_1 \bar{c}_1}{\bar{\rho}_2 \bar{c}_2} \\ \dfrac{1 - \bar{M}_1}{1 + \bar{M}_1}\left(\dfrac{1 + \gamma \bar{M}_1}{\gamma - 1} + \bar{M}_1^2 - \bar{M}_1^2 (1 + \bar{M}_1)\tfrac{1}{2}\left(\dfrac{\bar{u}_2^2}{\bar{u}_1^2} - 1\right)\right) & -\dfrac{\bar{c}_2}{\bar{c}_1}\,\dfrac{(1 - \gamma \bar{M}_2)}{\gamma - 1} - \bar{M}_1 \bar{M}_2 \dfrac{\bar{\rho}_1}{\bar{\rho}_2} \end{pmatrix}.$$

REFERENCES

Awad, E. & Culick, F. E. C. 1986 *Combust. Sci. Tech.* **46**, 195–222.

Bloxsidge, G. J., Dowling, A. P., Hooper, N. & Langhorne, P. J. 1988*a* *AIAA J.* **26**, 783–790.

Bloxsidge, G. J., Dowling, A. P. & Langhorne, P. J. 1988*b* *J. Fluid Mech.* **193**, 445–473.

Chu, B. T. 1964 *Acta Mechanica* **1**, 215–234.

Culick, F. E. 1988 *AGARD CP* 450.

Dowling, A. P. 1995 *J. Sound Vib.* **180**, 557–581.

Flandro, G. A. 1985 *AIAA J. Propulsion* **1**, 210–221.

Fleifil, M., Annaswamy, A. M., Ghoniem, Z. & Ghoniem, A. F. 1996 *Combust. Flame* **106**, 487–510.

Greitzer, E. M. 1976 *Trans. ASME J. Engng for Power* **98**, 190–217.

Gulati, A. & Mani, R. 1990 *AIAA Paper* 90-0270.

Heckl, M. A. 1988 *J. Sound Vib.* **124**, 117–133.

Hedge, V. G., Reuter, D. & Zinn, B. T. 1988 *AIAA J.* **26**, 532–537.

Kailasanath, K., Gardner, J. H., Oran, E. S. & Boris, J. P. 1991 *Combust. Flame* **86**, 115–134.

Keller, J. O., Vaneveld, L., Korschelt, D., Hubbard, G. L., Ghoniem, A. F., Daily, J. W. & Oppenheim, A. K. 1982 *AIAA J.* **20**, 254–262.

Kwong, A. H. M. & Dowling, A. P. 1994 *Trans ASME: J. Fluids Engng* **116**, 842–847.

Langhorne, P. J. 1988 *J. Fluid Mech.* **193**, 417–443.

Langhorne, P. J., Dowling, A. P. & Hooper, N. 1990 *AIAA J. Propulsion* **6**, 324–333.

Lores, M. E. & Zinn, B. T. 1973 *Combust. Sci. Tech.* **7**, 245–256.

McIntosh, A. C. 1991 *Combust. Sci. Tech.* **75**, 287–309.

Macquisten, M. A. & Dowling, A. P. 1993 *Combust. Flame* **94**, 253–264.

Macquisten, M. A. & Dowling, A. P. 1995 *J. Sound Vib.* **188**, 545–560.

Ogata, K. 1970 *Modern Control Engineering*. Prentice-Hall.

Pitz, R. W. & Daily, J. W. 1981 *AIAA 19th Aerospace Meeting*.

Poinsot, T., Bourienne, F., Candel, S. & Esposito, E. 1989 *AIAA J. Propulsion* **5**, 14–20.

Poinsot, T. & Candel, S. M. 1988 *Combust. Sci. Tech.* **61**, 121–153.

Poinsot, T., Trouve, A. C., Veynante, D. P., Candel, S. M. & Esposito, E. 1987 *J. Fluid Mech.* **177**, 265–293.

Rayleigh, Lord 1896 *The Theory of Sound*. Macmillan.

Schadow, K. C. & Gutmark, E. 1992 *Prog. Energy Combust. Sci.* **18**, 117–132.

Schadow, K. C., Wilson, R. J. & Gutmark, E. 1988 *AIAA J.* **25**, 1164–1170.

Segawa, Y. 1980 *JSME Intl J.* **30**, 1443–1449.

Sivasegaram, S. & Whitelaw, J. H. 1987 *Combust. Flame* **68**, 121–130.

Smart, A. E., Jones, B. & Jewel, N. T. 1976 *AIAA Paper* 76-141.

Smith, D. A. & Zukoski, E. E. 1985 *AIAA Paper* 85-1248.

Sterling, J. D. & Zukoski, E. E. 1987 *AIAA Paper* 87-0220.

Tien, J. S. 1984 *Prog. Astro. Aero.* **90**, 791–840.

Wicker, J. M., Yoon, M. W. & Yang, V. 1995 *J. Sound Vib.* **184**, 141–171.

Yamaguchi, S., Ohiwa, N. & Hasegawa, T. 1985 *Combust. Flame* **62**, 32–41.

Yoon, W. S. & Chung, T. J. 1994 *J. Acoust. Soc. Am.* **96**, 1096–1103.